The dependence of magnetic coupling on growth direction in epitaxial Dy-Y superlattices



1989 J. Phys.: Condens. Matter 1 5997

(http://iopscience.iop.org/0953-8984/1/34/016)

J. Phys.: Condens. Matter 1 (1989) 5997–6003. Printed in the UK

LETTER TO THE EDITOR

# The dependence of magnetic coupling on growth direction in epitaxial Dy–Y superlattices

C P Flynn†, F Tsui†, M B Salamon†‡, R W Erwin‡ and J J Rhyne‡

† Department of Physics and Materials Research Laboratory, University of Illinois at Urbana-Champaign, 1110 W Green Street, Urbana, IL 61801, USA

‡ National Institute of Standards and Technology, Gaithersburg, MD 20899, USA

Received 15 June 1989

**Abstract.** Epitaxial superlattices of Dy and Y, grown by molecular beam epitaxy with modulation along the HCP *b* axis, fail to develop long-range magnetic order along ***b*** even for Y spacer layers of only nine atomic planes. The difference between these samples and *c*-axis superlattices reflects the highly anisotropic magnetic response of the Y interlayers.

Rare-earth (RE) metals and alloys develop complicated magnetisation waves which have been the object of much study [1]. Both longitudinal and transverse (helical) waves occur with quite long wavelengths, $\simeq$20 Å. They arise from peaks in the wavevector-dependent conduction electron susceptibility $\chi(\boldsymbol{q})$ for $\boldsymbol{q}$ along the $c^*$ axis of the HCP RE lattice [2]. These peaks are identified with wavevectors $\boldsymbol{q}_0$ that span nearly two-dimensional (2D) nesting features of the RE Fermi surface (FS). They result from a near-instability of the electron liquid to the formation of a spin-density wave characterised by $\boldsymbol{q}_0$. While the theory of these effects is quite well developed [2], it falls short of being fully quantitative mainly because the REs have complicated electronic structures [2, 3]. Recent experiments have added to this understanding by probing spin–spin interactions in single-crystal superlattices (SLs) synthesised from the heavy REs Gd [4], Dy [5], Er [6], and Ho [7] interleaved with 'non-magnetic' Y. In all investigations reported to date, samples were grown along the *c* axis so that the magnetic wavevector is parallel to the growth direction. These materials exhibit magnetisation waves, including the chirality of helical waves, that propagate through intervening Y layers [8] as thick as 120 Å, to create new 3D magnetic structures. In this Letter, we report studies of SLs and films grown along the HCP *b* axis [9] so that the magnetic wavevector lies in the growth plane. The results differ strikingly from those for *c*-axis materials. They reveal the conduction band anisotropy of the Y inter-layer, and point to the possibility of probing the orientation dependence of magnetic coupling using designed materials.

This Letter describes the results of neutron scattering experiments on *b*-axis single-crystal Dy/Y SLs and Dy films. The samples were prepared by molecular beam epitaxy, as described elsewhere [9], on single-crystal Y substrates cut and polished at the Ames Laboratory. In this orientation the crystal surfaces are often badly reconstructed, so the interfaces of the SLs may be somewhat rougher than in *c*-axis samples, although the coherence of the crystal structure remains excellent. Neutron scattering studies of the magnetic and lattice structures were carried out on a triple-axis spectrometer at the

0953-8984/89/345997 + 07 $02.50  

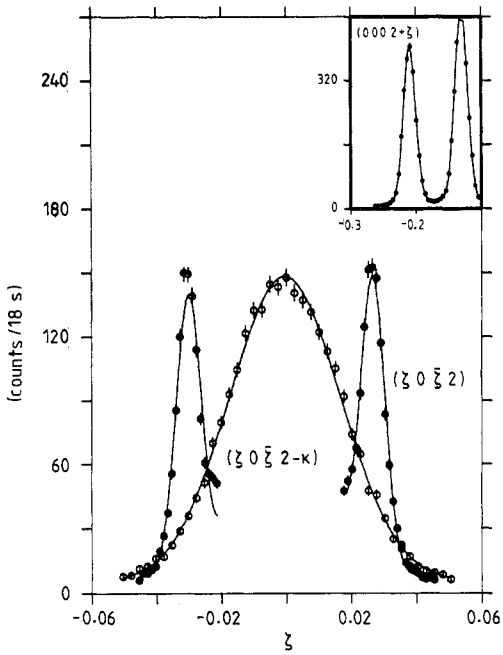


**Figure 1.** Magnetic and structural peaks of the *b*-axis superlattice $[Dy_{26}|Y_9]$. Open circles: scan along $\boldsymbol{a}^*$ across magnetic peak at $(0\,0\,0\,2-\kappa)$; full circles: scans through $(0\,0\,0\,2)$ along $\boldsymbol{a}^*$ in a field of 2.5 T to show the structural satellites of $(0\,0\,0\,2)$. Inset: comparable scan through a magnetic group of the *c*-axis SL $[Dy_{16}|Y_9]$ showing long-range multi-layer order.

National Institute of Standards and Technology Reactor. A graphite analyser crystal, set for zero energy transfer, was used to reduce the background from neutrons inelastically scattered by the thick Y substrates. We focus here on three aspects of the data: the magnetic transitions in the Dy layers, the magnetic coherence of the resulting structures, and the degree to which 3D order occurs. The results from three samples are described. Two are SLs: $[Dy_{26}|Y_9]_{82}$ (26 Dy planes and 9 Y planes, repeated 82 times), and $[Dy_7|Y_{25}]_{67}$; the third is a 350 Å *b*-axis Dy film.

The proximity of the average lattice parameter of the SL to that of the Y substrate prevented direct observation of the (0002) SL Bragg peak. Its location was therefore inferred from the positions of the (0002) magnetic satellites. The satellites were observed below $T_N = 170$ K at $(0\,0\,0\,2 \pm \kappa)$, as expected for a basal plane spiral along $\boldsymbol{c}^*$ with wavevector $\boldsymbol{q}_0 = \kappa \boldsymbol{c}^*$. Figure 1 shows one such peak for $[Dy_{26}|Y_9]_{82}$ at 6 K, with $\kappa = 0.204$ and $\boldsymbol{c}^* = 1.111$ Å$^{-1}$. This scan passes along the $\boldsymbol{a}^*$ reciprocal-lattice direction, parallel to the growth axis, with $\zeta$ the scan variable. From the peak width $\delta Q_{a^*} = 0.078$ Å$^{-1}$ we estimate a coherence length along the *b* axis of

$$\xi_b = 2\pi/[(\delta Q_{a^*})^2 - \Delta^2]^{1/2} \simeq 80 \text{ Å} \tag{1}$$

with $\Delta = 0.017$ Å$^{-1}$ the intrinsic width of the nuclear Bragg peaks (see below). This is very close to the $\xi_b = 73$ Å that would be expected if each Dy layer were to order independently. Similar results obtained for the $[Dy_7|Y_{25}]_{67}$ SL yield $\xi_b \simeq 40$ Å, if the same $\Delta$ is assumed, as compared with the 20 Å thickness of the Dy layers. Furthermore, the absence of resolvable peaks at $(\delta\,0\,\bar{\delta}\,2-\kappa)$, with $\delta = \pm 2\pi/La^*$, L the superlattice period, and $a^* = 1.980$ Å$^{-1}$, establishes that successive Dy layers do not order into a coherent 3D structure. This important observation points to a sharp distinction between long-range magnetic coupling in the *b*-axis and *c*-axis directions. An example inset to figure 1 shows magnetic satellites for a $[Dy_{16}|Y_9]_{100}$ *c*-axis SL, with widths that correspond to magnetic coherence extending over many SL periods. Thus, while Dy layers in *c*-axis

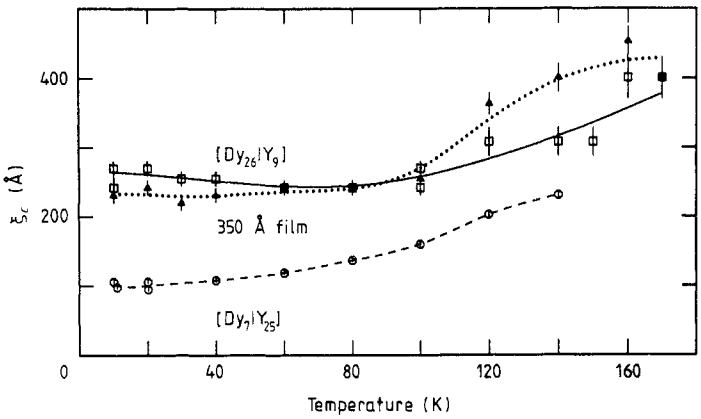


**Figure 2.** The variation of the coherence length $\xi_c$ along (0 0 0 2) with temperature. The coherence length in the (1 1 $\bar{2}$ 0) direction is comparble to the structural coherence.

SLs couple together across Y-layer spacing exceeding 120 Å [8], the Dy layers in *b*-axis samples order independently down to spacings of 26 Å.

That the samples possess good chemical coherence is most conveniently demonstrated by scanning the SL harmonics of the (0 0 0 2) Bragg peak in the presence of a 2.5 T field applied along the easy *a* axis. The field drives the Dy layers ferromagnetic, thereby increasing the scattering contrast with Y. Data from scans through (0 0 0 2) along $\boldsymbol{a}^*$ are superimposed on the magnetic satellite data in figure 1. The full width of the structural harmonics is $\Delta = 0.017$ Å$^{-1}$, while instrumental resolution is 0.010 Å$^{-1}$. The ferromagnetic coherence extends over the entire sample, as indicated by the vanishing of the helical satellite peaks and by auxiliary measurements of the saturation magnetisation. Therefore $\Delta$ measures the mosaic width and structural regularity of the multi-layer. It is used in (1) to calculate the magnetic coherence length. We conclude that the considerable width of the magnetic peaks reflects the limited magnetic coherence length $\xi_b$, not irregularity of the crystal structure.

The *b*-axis SLs with thick and thin Dy layers exhibit quasi-two-dimensional order below 175 K and 150 K, respectively. The thin Dy film also orders near 175 K, and with $\xi_b \geqslant 250$ Å, comparable with its 350 Å thickness. In the $[Dy_{26}|Y_9]_{82}$ sample, the width of the magnetic peak along (1 1 $\bar{2}$ 0) (i.e., along the *a* axis in the growth plane) is independent of temperature and comparable to $\Delta$, which corresponds to $\xi_a \geqslant 500$ Å. However, $\xi_c$ is significantly smaller, and it decreases with decreasing temperature as shown in figure 2. The magnetic order therefore consists of ferromagnetic sheets that are uniform across the *a*–*b* plane of each Dy layer, and stacked coherently over a temperature-dependent domain size along the *c* axis. A similar $\xi_c(T)$ was observed in the 350 Å film, as was a shorter and even more pronounced temperature dependence in $[Dy_7|Y_{25}]_{67}$ (see figure 2). Note that none of the *b*-axis samples exhibits the spontaneous ferromagnetic order of bulk Dy, at least above 5 K, and that the turn angles $\omega = \pi\kappa$ are less dependent on temperature than in bulk Dy, as shown in figure 3. In the $[Dy_7|Y_{25}]_{67}$ SL the turn angle actually increases with decreasing temperature (in contrast to bulk Dy) to a value that exceeds that of bulk Dy (43° at $T_N = 176$ K) [10]. The satellite position gives $\omega$ directly in the *b*-axis geometry, since no phase advance across the Y layers occurs as in the *c*-axis case.

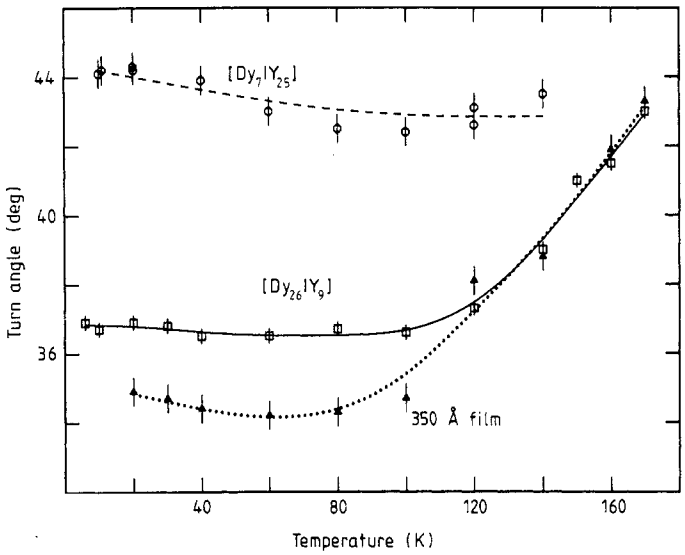


**Figure 3.** The temperature dependence of the spiral turn angle of *b*-axis multi-layers and films. Bulk Dy reaches a value of 25° at $T_C = 88$ K.

In second-order perturbation theory (i.e., linear response), the conduction electrons react to small magnetic perturbations with a $q$-dependent linear susceptibility $\chi(q)$ [2, 11, 12]. Two magnetic ions with spins $S_1$ and $S_2$, at $r_1$ and $r_2$ are then coupled by a Hamiltonian $\mathcal{H} = -S_1 \cdot S_2 J(R)$, in which $R = r_2 - r_1$ and

$$J(R) = \sum_q j(q)\, e^{-iq\cdot R} \tag{2}$$

with $j(q) = |j_{sf}(q)|^2 \chi(q)/2$ and $j_{sf}(q)$ is the exchange matrix element connecting band states to the 4f core [2, 11]. For an isotropic electron gas $J(R)$ takes the well known RKKY form $\sim\cos(2k_F R)/(k_F R)^3$, but in the present application the particular spatial form of $J(R)$ for the REs is needed (see below). The interaction must be summed over all pairs to obtain the energy. Note that detailed electronic processes such as scattering, or the sharing of a common FS among the layers of a SL, enter only through their effect on $J(R)$. This approach remains valid for small changes about the mean even when the summed interactions exceed the linear regime; thus, ordering near equilibrium may be treated. When perturbations are clustered, for example, with the result that the material is no longer homogeneous, linear response theory still holds, but $J(r_1, r_2)$ depends explicitly on $r_1, r_2$ rather than $R = r_2 - r_1$ alone. In the SLs of interest here, however, the actual differences between the susceptibilities $\chi(q)$ in (2) of Y and Dy are known to be quite small. The effect of inhomogeneity is therefore neglected in the following approximate account.

For Dy and Y in the SLs studied here, it is well documented that $j(q)$ has peaks along $c^*$ that arise from almost 2D sheets of nesting hole FS. Along $a^*$ and $b^*$, $j(q)$ falls off in a way that mainly reflects the core size, and may be represented [12] by a Gaussian of width 0.63 $Å^{-1}$ (a faster fall may occur when $q$ exceeds the span of the hole FS, but this is not significant here). The peaks along $c^*$ are more difficult to model accurately. They differ somewhat between Y and Dy, and even more among different theories for Y [12,

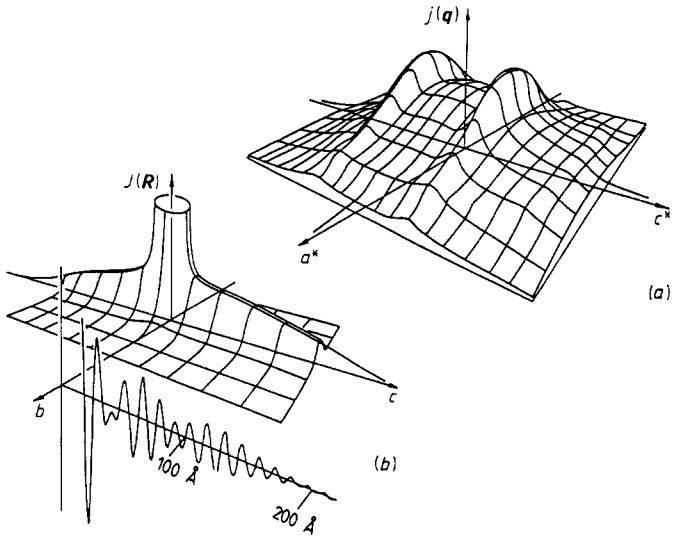


**Figure 4.** (*a*) A schematic representation of $j(\boldsymbol{q})$. The width along $\boldsymbol{a}^*$ is determined mainly by the $j_{sf}(\boldsymbol{q})$ element while that along $\boldsymbol{c}^*$ fits sharp features in $\chi(\boldsymbol{q})$. (*b*) A sketch of the envelope function of the Fourier transform of the $j(\boldsymbol{q})$ in (*a*), showing the anisotropic spatial extent. Also shown is the actual oscillatory Fourier transform $J(\boldsymbol{R})$ of Liu's $j(\boldsymbol{q})$ along the *c* axis [13].

13]. Liu [13] finds a peak $\simeq 0.7j(0)$ high with a markedly square top and structure $\simeq 0.03$ Å$^{-1}$ wide. The general features of $j(\boldsymbol{q})$ are sketched in figure 4(*a*). According to (2), $J(\boldsymbol{R})$ is the Fourier transform of $j(\boldsymbol{q})$, and its general envelope is sketched in figure 4(*b*), consistently with figure 4(*a*). Also shown there is the actual $J(\boldsymbol{R})$ along $\boldsymbol{c}$ calculated from Liu's results (Kasuya's give a similar range and wavelength, but $J(\boldsymbol{R})$ falls off without beats). Details will be provided in a later comprehensive article. The main feature that emerges unambiguously from these calculations is that $J(\boldsymbol{R})$ extends with significant amplitude for some 130 Å along $\boldsymbol{c}$, but falls off to the same strength in only 12 Å along $\boldsymbol{a}$ and $\boldsymbol{b}$.

Several aspects of the magnetic behaviour are clarified by this picture. For our present purpose the most important one is that the anisotropy of $J(\boldsymbol{R})$ explains in a natural way why magnetic layers in SLs couple at separations over 100 Å along $\boldsymbol{c}$ but fail to couple at 26 Å along $\boldsymbol{a}$ and $\boldsymbol{b}$. While the theory is not fully quantitative, both the ranges and the anisotropy are predicted reasonably well. Furthermore, since the susceptibility peaks and matrix elements are similar for Dy and Y, it is natural that these qualitative features should be preserved in the SL. It may also be recognised that the approximate interaction volume $260 \times 24 \times 24 \sim 10^5$ Å$^3$, or $>10^3$ neighbours, readily accounts for the observed ordering in Y alloys containing only a few atomic per cent of magnetic impurities [14]. Two further points are of interest. First, measurements on *a*-axis SLs give results similar to those for *b*-axis samples, as the description given above here would also suggest. Second, the lack of observed coupling along $\boldsymbol{a}$ and $\boldsymbol{b}$ lends confidence that the long range along $\boldsymbol{c}$ is not an artefact due to unknown structural flaws.

The ordering of the individual Dy epitaxial layers shows two major differences from bulk behaviour that are seen also in *c*-axis SLs. The principal effect is the complete suppression in films and SLs of the ferromagnetic transition that occurs at 85 K in the

bulk. A second is the much smaller decrease in the turn angle $\omega$ with decreasing temperature. While a fully quantitative treatment is still lacking, it is clear that both effects arise mainly from lattice 'clamping'. Specifically, as the epitaxy clamps the dimensions of the Dy growth plane to those of the Y substrate, the layers can no longer gain magnetoelastic energy from in-plane distortions; in principle, this creates a distinct magnetic phase diagram for each epitaxial orientation. Further discussion of these phenomena will appear in a detailed publication.

Finally, we discuss the unusual coherence properties of the *b*-axis Dy layers. The limited *b*-axis coherence is attributed above to the lack of inter-layer coupling, but the unusually short, temperature-dependent *c*-axis coherence (figure 2) still requires explanation. In all RE samples, exchange is ferromagnetic in the basal plane. This leads to long-range coherence in the *a* direction for SLs and in both *a* and *b* directions for the 350 Å film. However, figure 2 shows that $\omega$ depends strongly on film thickness at low temperatures. Variations in layer thickness may thus cause a temperature-dependent inhomogeneous broadening of the magnetic Bragg peak indistinguishable from a reduction of $\xi_c$. That *c*-axis coherence in *a*- and *b*-axis samples is limited and dependent on temperature, even in the 350 Å film, points to its origin in interfacial roughness, in interdiffusion, in dislocations or in a combination of these. The fact that the coherence deteriorates most dramatically in the temperature range where the turn angle is changing rapidly also supports this interpretation.

In summary, we have reported new results for the magnetic properties of *b*-axis RE SLs and films. It turns out that much of the behaviour can be rationalised on the basis of parameters for the pure metals. This modelling regards the SLs as successive layers that each respond just as in the bulk. Features of the coherence, the magnetic state and the inter-layer coupling can all be understood in approximate terms by these means. Not enough is yet known about the delicate energy balance of magnetic and magnetoelastic processes in the metals to determine how satisfactory such modelling may eventually be. A fact made evident by the present work is that the materials themselves can be designed and tailored to probe bulk behaviour such as anisotropy in new ways so that deeper insight may be forthcoming. One design currently being pursued in our work is intended to probe the detailed anisotropic spatial form of $J(\boldsymbol{R})$. From a broader perspective, it is nevertheless clear that electrons in multi-layers are to some degree shared among neighbouring metal layers, and that fundamental changes can only take place on the length scale of electronic relaxation, typically 10–50 Å. For thin layers or weak relaxation, neighbouring layers must share a common FS and exhibit corresponding changes of magnetic properties [11]. The present understanding of these interfacial phenomena is very limited even for simple metals. A challenge for the future is to create materials configurations that allow spatial variations of the connected Fermi systems of two neighbouring layers to be probed in a useful way.

We thank R Du and J Borchers for auxiliary characterisation of the samples, experimental assistance, and helpful discussions. This work was supported in part by NSF Grant DMR-86-21616 and by the National Institute of Standards and Technology. Use has been made of facilities of the Materials Research Laboratory, University of Illinois, funded by the NSF Grant DMR-86-12860. One of us (FT) thanks the IBM Corporation for fellowship support during this research.

## References

[1] Coqblin B 1977 *The Electronic Structure of Rare-Earth Metals and Alloys: the Magnetic Heavy Rare Earths* (London: Academic)

[2] Freeman A J 1972 *Magnetic Properties of Rare-Earth Metals* ed. R J Elliott (New York: Plenum) ch 6
Coqblin B 1977 *Magnetic Properties of Rare-Earth Metals* ed. R J Elliott (New York. Plenum) ch 9
[3] Evenson W E and Liu S H 1969 *Phys. Rev.* **178** 783
[4] Kwo J, McWhan D B, Gyorgy E M, Feldman L C and Cunningham J E 1985 *Layered Structures, Epitaxy and Interfaces* ed. J H Gibson and L R Dawson (Pittsburgh, PA: Materials Research Society) p 509
Majkrzak C F, Cable J W, Kwo J, Hong M, McWhan D B, Yafet Y, Waszczak J and Vettier C 1986 *Phys. Rev. Lett.* **56** 2700
[5] Erwin R W, Rhyne J J, Salamon M B, Borchers J, Sinha S, Du R, Cunningham J E and Flynn C P 1987 *Phys. Rev.* B **35** 6808
[6] Borchers J, Salamon M B, Du R, Flynn C P, Erwin R W and Rhyne J J 1988 *Superlatt. Microstruct.* **4** 439
[7] Majkrzak C F, Gibbs D, Boni P, Goldman A I, Kwo J, Hong M, Hsieh T C, Fleming R M, McWhan D B, Yafet Y, Cable J W, Bohr J, Grimin H and Chien C L 1988 *J. Appl. Phys.* **63** 3447
[8] Rhyne J J, Erwin R W, Borchers J, Salamon M B, Du R and Flynn C P 1987 *J. Appl. Phys.* **61** 4043
Hong M, Fleming R M, Kwo J, Schneemeyer L F, Waszczak J V, Mannaerts J P, Majkrzak C F, Gibbs D and Bohr J 1987 *J. Appl. Phys.* **61** 4052
[9] Du R, Tsui F and Flynn C P 1988 *Appl. Rev. B* **38** 2941
[10] Koehler W C 1972 *Magnetic Properties of Rare-Earth Metals* ed. R J Elliott (New York: Plenum) ch 3
[11] Yafet Y, Kwo J, Hong M, Majkrzak C F and O'Brien T 1988 *J. Appl. Phys.* **63** 3453
[12] Kasuya T 1966 *Magnetism* vol IIB, ed. G T Rado and H Suhl (London: Academic) ch 3
[13] Liu S H, Gupta R P and Sinha S K 1971 *Phys. Rev.* B **4** 1100
[14] Gotaas J A, Rhynn J J, Wenger L E and Mydosh J A 1987 *J. Appl. Phys.* **61** 3415